Toxicology and Applied Pharmacology 509 (2026) 117753

Contents lists available at ScienceDirect

Toxicology and Applied Pharmacology

journal homepage: www.elsevier.com/locate/taap

The effects of tungsten inhalation and continuous administration of angiotensin II on cardiac injury and pulmonary outcomes

Milad MazloumiBakhshayesh [a], Russell P. Hunter [a], Brenna Baird [a], Rui Liu [a], Anahi Gabriela Jimenez-Campos [a], Siem Goitom [a], Edward B. Barr [a], Guy W. Herbert [a], Selita N. Lucas [a], Charlotte M. McVeigh [a], Jorge Moreno [a], Yiliang Zhu [c], Barry E. Bleske [b], Matthew J. Campen [a], Alicia M. Bolt [a,*]

[a] Department of Pharmaceutical Sciences, The University of New Mexico, College of Pharmacy, Albuquerque, NM 87131, United States of America
[b] Department of Pharmacy Practice and Administrative Sciences, The University of New Mexico, College of Pharmacy, Albuquerque, NM 87131, United States of America
[c] Department of Internal Medicine, The University of New Mexico, School of Medicine, Albuquerque, NM 87131, United States of America

ARTICLE INFO

Editor: Lawrence Lash

Keywords:
Tungsten
Inhalation
Angiotensin II
Particulate Matter
Cardiac Injury
Cardiac Troponin I

ABSTRACT

Tungsten exposure is associated with multiple cardiovascular diseases, but limited information exists on the mechanistic underpinnings of these relationships. The current study investigated the individual and combined effects of angiotensin II (AT-II) treatment, as a model of accelerated cardiovascular disease risk, and tungsten (W) exposure on cardiac function, to provide insights into potential mechanisms involved in tungsten-mediated cardiac injury. Mice received AT-II (0.73 mg/kg/d) or saline (Veh) for 24 days through osmotic mini-pumps. The final 2-weeks of treatment, mice were exposed 4 times (4 h each) to filtered air (FA) or 1.50 ± 0.22 mg/m^3 W particles by whole-body inhalation. Laser ablation and bulk inductively-coupled plasma mass spectrometry (ICP-MS) of lung samples indicated an accumulation of iron in AT-II treatment groups and confirmed the deposition of W and decreases in essential elements zinc, magnesium, and molybdenum in exposure groups. Echocardiographic data showed W exposure decreased cardiac output and stroke volume; however treatment with AT-II did not further exacerbate W's effects. The A'/E' ratio was significantly elevated in the AT-II + W group compared to the W + Veh group and trending significant compared to the FA + AT-II group. Blood cardiac troponin I was elevated in the W + AT-II group compared to either FA + Veh or W + Veh groups. Results suggest an interactive effect of both W and AT-II to drive cardiac injury following exposure. However, neither W exposure nor AT-II treatment resulted in pulmonary inflammation at the terminal endpoint of the study. Data illustrate pathophysiological effects of inhaled W and AT-II that contribute to cardiac injury.

1. Introduction

Tungsten (W) is the 18th most abundant metal, having an estimated concentration in the earth's surface of 1–1.3 mg/kg. W is also a highly valuable element, due to its outstanding characteristics, including high melting point and density, exceptional tensile strength, flexibility, and excellent electrical conductivity, which had resulted in the use of tungsten in many different industrial products. In recent years, concerns have been raised due to increasing human exposure to W through multiple routes of exposure (Agency for Toxic Substances and Disease Registry, A, 2005). In occupational settings, exposure can occur through inhalation of dust particles and dermal contact during the production or processing of W-containing compounds. Notably, considerable amounts of W dust are released during ore processing, component mixing, and product shaping and grinding (Bolt and Mann, 2016; Keith et al., 2007; Kraus et al., 2001; Agency for Toxic Substances and Disease Registry, A, 2005). Ambient air concentrations of W in hard metal manufacturing facilities have been reported to range between 0.003 and 2.13 mg/m^3; (Kraus et al., 2001; Stefaniank et al., 2009). Human biomonitoring studies conducted in these facilities report urinary W concentrations ranging between 0.33 and 168.6 μg/g creatinine (parts per billion (ppb)) (Kraus et al., 2001). Another occupational cohort potentially at risk of exposure to high levels of W is military members who can be exposed though inhalation of W particles or embedded pieces of W metal

* Corresponding author at: Department of Pharmaceutical Sciences, MSC09 5360, 1 University of New Mexico, Albuquerque, NM 87131, United States of America.
E-mail address: ambolt@salud.unm.edu (A.M. Bolt).

https://doi.org/10.1016/j.taap.2026.117753
Received 23 October 2025; Received in revised form 29 January 2026; Accepted 2 February 2026
Available online 6 February 2026

shrapnel following detonation of ammunition or explosive devices containing W. W particulate concentrations following detonation of improvised explosive devices containing W detect ambient levels ranging between 3.7 and 8.95 mg/m^3, with 1.95–3.08 mg/m^3 being in the respirable fraction ($\leq$ 10 μm in size; (Machado et al., 2010)). In a recent survey of military veterans with embedded metal fragments, W was the second most commonly elevated metal found in the urine (range 0.003 to 2.70 μg/g creatinine) (Gaitens et al., 2017). However, it is not known what fraction of the W exposure in this cohort is due to inhalation exposure. In contrast, concentrations of W metal particles in the ambient air in the environment are much lower ($<$ 10 ng/m^3; (Dams et al., 1970; Haddad and Zikovsky, 1985; Jagielak and Mamont-Ciesla, 1979)). Urinary tungsten levels in the general population are quite variable ranging between 0.08 and 0.7 ppb (Paschal et al., 1998; Tyrrell et al., 2013; CDC, 2003; Health Canada, 2013). However, it is difficult to determine what fraction of these exposures is from inhalation of W particulates versus other sources of exposure.

Understanding W's properties, potential exposure pathways, and toxicity is crucial for assessing its impact on human health and the environment. Several epidemiological studies have reported that W exposure is associated with increased incidence and mortality of cardiovascular diseases and stroke. There are no studies directly linking W exposure with increased incidence or mortality from heart failure, but there are associations with increased risk of composite cardiovascular disease outcomes as well as precursor diseases that can lead to the development of heart failure such as hypertension (Agarwal et al., 2011; Nigra et al., 2018; Shiue and Hristova, 2014; Zhao et al., 2023). However, we do not have a clear understanding of the underlying molecular mechanisms linking W exposure to cardiovascular disease development.

Multiple *in vivo* studies have evaluated pulmonary toxicity following inhalation exposure to W particles. Studies indicates that chronic inhalation to W particles leads to pulmonary inflammation, fibrosis, and altered lung function (Lasfargues et al., 1992, 1995; Miller et al., 2021; Prajapati et al., 2017; Rajendran et al., 2012; Rengasamy et al., 1999; Roedel et al., 2012), However there is very limited data investigating the systemic consequences following inhalation exposure. Our group was the first to demonstrate that inhalation of W particles leads to cardiac injury in wildtype female Balb/c mice, including inflammation in the lungs and heart, reduced cardiac output, and early signs of diastolic dysfunction (Miller et al., 2021; Templeton et al., 2023). Hypertension is the leading cause of cardiovascular disease and premature death worldwide (Mills et al., 2020). High blood pressure is one of the most important risk factors for ischemic heart disease, stroke, other cardiovascular diseases, chronic kidney disease, and dementia (Fuchs and Whelton, 2020). An estimated 1.28 billion adults aged 30–79 years worldwide have hypertension, most (two-thirds) living in low- and middle-income countries (World Health Organization, n.d.). Evaluating the effects of W in the context of a mild hypertension model is relevant and will be able to point to potential mechanistic drivers of tungsten-mediated cardiac injury.

Two primary systems implicated in hypertension and subsequent cardiac remodeling include the sympathetic system and the renin–angiotensin–aldosterone system. The activation of these systems triggers intracellular signaling pathways that promote protein synthesis in both myocytes and fibroblasts (Azevedo et al., 2016). As myocytes stretch, local norepinephrine activity and angiotensin and endothelin release are increased (Cohn et al., 2000).

To follow up on the potential consequences in a vulnerable population, the present study examines the effects of W exposure with and without continuous administration of angiotensin-II (AT-II), which has vasopressor and cardiomyocyte mitogenic properties (Gonzalez-Villalobos et al., 2008; Peng et al., 2011). This study aims to investigate the effects of inhalation exposure to W metal particles and continuous administration of AT-II on cardiac injury in male BALB/c mice. We hypothesized that continuous administration of AT-II will further enhance cardiac injury and altered cardiac function following inhalation exposure to W particles. To test this primary hypothesis, this study used a 2 × 2 factorial design that enables the investigation of both individual and combined effects of AT-II treatment and W exposure. This study will provide important insight into the underlying mechanisms driving tungsten-mediated cardiac injury and altered cardiac function.

2. Materials and methods

2.1. Animal study design

24 male BALB/cAnNCrl (BALB/c) mice (purchased from Charles Rivers Laboratories, Wilmington, MA, USA – CRL:028), aged 4–6 weeks were divided into four different groups: Group 1: filtered air (FA) + vehicle (Veh; saline, NaCl 0.9%; FA + Veh), Group 2: W + Veh (1.50 ± 0.22 mg/m^3), Group 3: FA + AT-II, and Group 4: W + AT-II (1.50 ± 0.22 mg/m^3). Of note one mouse in the FA + AT-II group died at implantation of the osmotic minipump so this mouse was excluded from the study. All animal experimental protocols received approval from the Institutional Animal Use and Care Committee (IACUC) at the University of New Mexico Health Sciences Center (Approved IACUC Protocols 25–201673-HSC and 22–201308-HSC). Mice had access to water and food ad libitum with a 12 h light: dark cycle and were housed in an AAALAC-accredited animal husbandry facility. Mice were feed a standard chow diet (Teklad 2920×). Male BALB/c mice were chosen for this study to build off of our previous study performed in female BALB/c mice, to be able to make conclusions on sex-specific differences in cardiac injury and pulmonary responses following inhalation exposure to tungsten particles between male and female mice.

The study duration was 31 days (Fig. 1), with the initial 7 days dedicated to the acclimation of the mice. All mice were implanted with osmotic mini pumps (technique described below) containing AT-II or Veh and treated for 24 days. At day 21, pre-exposure cardiac function was evaluated using echocardiography (technique described below). Mice were then exposed to FA or W by whole body inhalation on days 22, 24, 26 and 29 (technique described below). At day 30 post-exposure cardiac function was evaluated using electrocardiography. At the terminal endpoint, at day 31, bronchoalveolar lavage fluid (BALF) was collected (technique described below), and mice were immediately euthanized using approved methods of cardiac exsanguination followed by cervical dislocation. For all procedures requiring anesthesia, mice were anesthetized with continuous administration of 3–5% isoflurane in O_2

2.2. Implantation of osmotic mini-pump

Osmotic mini-pumps (model 1004; Alzet, Cupertino, CA, USA) were used in this study to provide continuous AT-II or Veh delivery for the 24 days of the study. Use of osmotic mini-pumps is a validated and reliable method for continuous administration of AT-II (Colombo et al., 2013; Almoshari, 2022) Twelve pumps were filled with AT-II (Sigma-Aldrich, St. Louis, MO, USA, Catalog Number: A9525) at a concentration designed to deliver 0.73 mg/kg/d and the remaining 12 were filled with saline (NaCl 0.9%); pumps were primed overnight in sterile saline prior to implantation. The renin-angiotensin-aldosterone system is a multifaceted hormonal cascade central to cardiovascular and renal homeostasis. This intricate system initiates the production of renin in the kidney, its interaction with angiotensinogen, and the formation of angiotensin I, which is then converted into the potent vasoconstrictor AT-II by angiotensin-converting enzyme (ACE). AT-II acts on receptors, notably AT1R and AT2R, to regulate blood pressure and fluid balance. This concentration of AT-II is 50% lower than the concentration that has been shown to induce hypertension and cardiomyocyte hypertrophy in BALB/c mice (Peng et al., 2011).

Briefly, pump implantation was conducted using aseptic procedures. Mice were anesthetized with continuous administration of 3–5% isoflurane in O_2. A small incision was made subcutaneously near the

Fig. 1. Study period and design.

scapulae. A small opening was made in the subcutaneous layer using blunt dissection and the mini-pump was gently inserted subcutaneously. The wound was closed using surgical clips. Topical lidocaine at the site of incision was used as an analgesic. Daily wound checks were conducted to monitor for signs of infection or other issues, which would be promptly reported to the veterinarian. After a week, the clips were removed from the wound. The weight of each mouse was >20 g (exceeding the minimum weight requirement necessary for implantation) with an average weight at implantation of 21.6 g. During the acclimation period, a dietary supplement (diet gel 76 A, Clear H_2O, Westbrook, ME, USA) was placed in the cage to facilitate weight gain in the mice post-surgery. Treatment with AT-II did not result in overt toxicity including no changes in total body weight (Supplemental Fig. 1).

2.3. Tungsten Exposure

Particulates of pure elemental W (99% elemental purity, particulate size distribution 1–5 μm in diameter) were purchased from Alfa Aesar (Haverhill, MA, USA; Catalog Number: 01040036; CAS Number: 7440-33-7). These W particles have been comprehensively characterized previously (Miller et al., 2021; Templeton et al., 2023), using both a laser aerosol spectrometer (model 3340 A; TSI) and scanning electron microscopy. The exposure system enriches for W particulates <1 μm in diameter (Count Mean Diameter; CMD), presumably due to the prolonged suspension time for smaller particles. The average CMD over multiple exposures was 0.4 ± 0.02 μm in diameter (Templeton et al., 2023). The average Geometric Standard Deviation (GSD) was 1.8 ± 0.16 and the average Mass Mean Diameter (MMD) was 1.2 ± 0.37 μm in diameter, which is within the particle size range reported by the manufacturer (Templeton et al., 2023). This particulate size is in the respirable fraction of particles and is relevant to occupational exposures where individuals are consistently exposed to respirable sized particles (< 10 μm in size) including fine particles (< 2.5) that can travel into the deep lungs (Klasson et al., 2016; McKernan et al., 2009; Day et al., 2009).

The whole-body inhalation exposure system has been published previously (Miller et al., 2021; Templeton et al., 2023). In summary, a fluidized bed aerosol generator (model 3340; TSI; Shoreview, MN, USA) introduced a continuous stream of particulates into the chamber while maintaining an exhaust flow rate. W particulate exposure concentrations were assessed in real-time using a DustTrak DRX monitor (model 8533; TSI), with results reported as a voltage output to LabVIEW Software (National Instruments, Austin, TX, USA). LabVIEW Software translated the voltage into an estimated aerosol concentration of W particulates. Actual aerosol concentrations were determined gravimetrically by taking four filter samples during each of the 4-h exposure periods. Across the four x 4-h exposures spanning the 8 day timeframe, the average air concentration of W particles ± standard deviation (SD) was measured at 1.50 ± 0.22 mg/m^3. This exposure model represents an occupational exposure where individuals are repeatably exposed to W particles over the course of multiple days. The average particulate concentration over the course of each single 4-h exposures was 1.49, 1.44, 1.22, and 1.85 mg/m^3. Exposure to W particles did not result in overt toxicity including no changes in total body weight (Supplemental Fig. 1).

2.4. Echocardiography

Echocardiography, a non-invasive imaging modality was employed to evaluate cardiac morphology and function. Echocardiography was performed in a blinded manner by a trained sonographer (MJC) using an ultrasound system equipped with a 21 MHz linear array transducer (Vevo LAZR-X 3100, Fujifilm, VisualSonics, Toronto, ON, Canada). Mice were anesthetized with continuous administration of isoflurane (3–5%) in an O_2 carrier; heart rate was monitored in real-time and anesthesia depth was adjusted as needed to ensure that the heart rate was at or above 500 bpm (Hartley et al., 2008; Roth et al., 2002; Wikström et al., 2008). Two-dimensional M-mode, and tissue doppler imaging were obtained according to standard protocols, averaged from at least five consecutive heartbeats from 4 separate images of the M-Mode cardiac view, taken for each animal. Software (Vevo LAB, Fujifilm) from the ultrasound instrument was used to measure parameters such as left ventricular (LV) end-diastolic and end-systolic dimensions. Tissue doppler imaging was utilized to assess the motion of the left ventricular free wall.

2.5. Bronchoalveolar lavage fluid for immune cell profiling

BALF was collected as previously described (Miller et al., 2021; Templeton et al., 2023). Briefly, mice were anesthetized with continuous administration of 3–5% isoflurane in O_2. Mouse tracheae were intubated with a 20-guage cannula. 1 mL 1× Dulbecco's phosphate buffered saline (dPBS; Thermofisher Scientific, Waltham, MA, USA) was used to inflate the lungs and BALF as removed using a 1 mL syringe. The collected BALF was processed within 24 h to prevent cell degradation, as delaying beyond this timeframe could compromise cell count accuracy. Cell counts were determined using trypan blue dye and a 1:5 dilution on a hemacytometer. All five hemacytometer regions were counted, excluding red blood cells based on their concave centers. The total cell count from these calculations determined the required BALF volume for 100,000 cells. Cytospin slides were created using the Shannon cytospin system, labeled appropriately, and placed in cytospin funnels with filter paper. Slides underwent centrifugation at 800 rpm for 5 min, followed by air drying in a flat position. After complete drying, slides were stained with Diff-Quik or similar stain, following instructions to ensure complete dryness before examination.

2.6. Terminal blood collection

Immediately following BALF collection, blood (unfasted) was collected from each mouse using cardiac puncture of the left ventricle. A small portion of blood (~100 μL) was directly transferred to the sample well of the iStat™cartridge for measurement of Cardiac Troponin I (CTnI).

2.7. Tissue Collection

Following BALF collection and exsanguination the lungs were inflated with optimal cutting temperature (OCT) compound (Scigen Scientific Gardena, Ca, USA /Fisher HealthCare, Houston, TX, USA), after which lungs and heart were collected in collecting tubes. These tubes were then transferred to dry ice for preservation and subsequently stored in a − 80 °C freezer. Blood samples were promptly utilized for the measurement of cardiac troponin I by using the i-Stat device.

2.8. Rapid Cardiac Troponin I Testing with i-stat

CTnI cartridges (B23032A) were sourced from Abbott Point-of-Care Inc., Chicago, IL, USA. ~100 μL of whole blood was directly transferred to the sample well of the iStat™cartridge for analysis according to manufacturer's instructions. The cartridges were analyzed using the i-STAT 1 analyzer, handheld instrument. This is a validated rapid, point of care method to measure CTnl in mouse blood (Dries et al., 2011). Concentrations of CTnl in blood are directly displayed on the analyzer screen (ng/mL). The i-STAT 1 system runs a comprehensive set of internal controls for proper quality assurance and quality control for both the analyzer and cartridge performance each time a sample is run.

2.9. Bulk Inductively-Coupled Plasma Mass Spectrometry (ICP-MS)

The concentrations of metals in the lungs were determined using bulk Inductively Coupled Plasma-Mass Spectroscopy (ICP-MS) with an Agilent 7900 instrument (Agilent Technologies, Santa Clara, CA, USA), which was coupled with an SPS 4 autosampler. Prior to acid digestion, lung tissue weights were recorded according to the sample type. Acid digestion was performed utilizing a heat block digester with 70% trace metal grade nitric acid (Aristar Plus grade, BDH). The samples underwent gradual heating (ramp and hold) to 95 °C for 2 h during digestion. Following digestion, the samples were normalized to a total volume of 10 mL using 18 M-ohm water before the ICP-MS analysis. The limit of detection for metal was 0.050 ppb.

The ICP-MS instrument was calibrated and optimized by a multi-element tuning solution across a wide mass range standard. All measurements were performed in triplicate and in helium mode. Solutions were prepared using 2% nitric acid to match the standards matrix. Calibration was executed with blank and five standards. For data validation and verification, samples were analyzed along with quality control samples. Moreover, in each experimental sample batch, a Continuing Calibration Verification quality control sample was included, and it was analyzed after every ten samples to further confirm the calibration and stability of the instrument. The obtained data were reported as the mean metal concentration per gram of tissue weight (ng/g - ppb).

2.10. Embedding tissue on OCT and Slicing Tissue for Laser Ablation

Lung tissue samples were embedded in cryomolds and filled with optimal cutting temperature (OCT) compound (purchased from Fisher Health Care, Waltham, MA, USA). The cryomolds were then carefully placed on dry ice, which had been treated with pure ethanol to facilitate evaporation. This freezing process was executed in a manner that ensured the tissue and OCT inside the cryomolds remained uncontaminated by dry ice and ethanol. Contamination of the OCT could lead to gelation, which is undesirable for sectioning and may result in the sample falling from the mold holder during the process. Subsequently, the cryomolds were wrapped in aluminum foil and stored in a − 80 °C freezer for a period of 24 h.

Following the 24-h freezing period, the frozen OCT containing the specimen was separated from the cryomolds. A small amount of OCT was applied to a mold holder, onto which the sample was carefully positioned. The mold holder, with the sample securely in place, was then affixed to a specialized sectioning device designed for freezing and connecting the mold holder and the specimen. After a 10-min interval, the sectioning procedure commenced using a microtome blade (procured from Accu-Edge) with sectioning device (Leica CM1860).

Slicing continued until reaching the tissue region of interest. To prevent folding of the slices, a camel hairbrush was used to unwrap the slices. Slice size was 20 μm, each slice was transferred to a slide, and after an additional 10-min interval, any excess frozen OCT was removed from the slides. Finally, the slides were placed in a slide box and stored in a refrigerator.

2.11. Laser Ablation ICP-MS (LA-ICP-MS)

In these experiments, an imageBIO266 laser ablation system (Elemental Scientific Lasers, Bozeman, MT, USA) with specific parameters including a 266 nm wavelength, 7 J/cm2 energy fluence, 10 Hz repetition rate, 50 μm spot size, 500 μm/s scan speed, and a helium (He) carrier gas flow rate of 0.8 L/min, was utilized. This system was coupled with a Dual Concentric Injector (DCI) connected to an Agilent 7900 ICP-MS equipped with an RF power of 1550 W, a nebulizer gas (Ar) flow rate of 0.44 L/min, a dwell time of 10 ms, and the analysis of isotopes including 56Fe, 63Cu, 111Cd, and 182 W.

Prior to analysis, solid samples underwent meticulous cleaning to remove contaminants and were securely mounted on a holder to ensure stability during ablation. Calibration of the ICP-MS system using suitable standards was performed to guarantee accurate quantification, and the proper functioning of the ICP-MS was verified.

The laser ablation system was configured by customizing parameters such as laser energy, spot size, and ablation rate to match the sample's characteristics. During the ablation process, the sample holder was positioned within the laser ablation system, with precise laser focusing on the targeted area of the sample's surface. The resulting ablated material was efficiently transported to the ICP-MS using helium as the carrier gas. Within the ICP-MS, the ablated material was ionized through the inductively coupled plasma, followed by the separation of ions based on their mass-to-charge ratio and subsequent detection using the mass spectrometer. Signal intensities of detected ions were continuously monitored, providing insights into the elemental concentrations within the sample.

Specialized software facilitated the interpretation of mass spectra and the calculation of element concentrations in the ablated samples. Comparison of signal intensities of sample elements to calibration standards enabled precise determination of concentrations. To ensure measurement accuracy, National Institute of Standards and Technology reference materials were incorporated into the analysis, and replicate analyses were conducted to assess measurement precision.

2.12. RNA Isolation and Quantification of Gene Expression in Left Ventricle Heart Tissue by Real-Time Quantitative Polymerases Chain Reaction PCR (qPCR)

RNA was isolated from left ventricle hear tissue and gene expression in left ventricle heart tissue was quantified by real-time qPCR as previously described (Templeton et al., 2023). Briefly, total messenger RNA (mRNA) was isolated from left ventricle heart tissue using the RNeasy Mini Kit (Qiagen, Germantown, MD, USA) following manufacturer's protocol. Equal amount of RNA was reversed-transcribed using the High Capacity cDNA Reverse Transcription Kit (Applied Biosystems, Foster City, CA, USA) using the manufacturer's protocols. cDNA was amplified with real-time qPCR for a reference gene and multiple target genes using the LightCycler 480 Instrument II (Roche, Basel Switzerland) and Quant Studio Pro 7 (Applied Biosystems) instruments. Pre-designed and validated primer were purchase as Taqman Gene Expression Assays (Applied Biosystems). Genes of interest were *Acta-2* (Mm01546133_m1), *Col1α1* (Mm00801666_g1), *Col3α1* (Mm00802296_g1), *Tgf-β1* (Mm01178820_m1), *Tgf-β2*

(Mm00436955_m1), *Tnf-α* (Mm00443258_m1), and *Il-1β* (Mm00434228_m1). Gene expression data was normalized to the housekeeping gene *Gapdh* (Mm99999915_g1). Samples were analyzed in duplicate. Fold changes in gene expression were calculated by the $2^{-\Delta\Delta Ct}$ comparative threshold model using the FA + Veh groups as a reference.

2.13. Statistical analysis

GraphPad Prism v 10.0.03 (Boston, MA, USA) and R(4.3.2) software were used to summarize measurements and conduct statistical comparisons. Continuous variables were presented as mean ± SD. While two-way ANOVA is applicable to our 2 × 2 experiment of W (vs FA) and treatment (AT-II vs Veh), it is less specific to our study hypotheses. For example, the main effect of W in a two-way ANOVA compares the average value under W across both Veh and AT-II with the overall average, whereas we are specifically interested in differential effects of W under Veh and AT-II conditions separately. Therefore, we analyzed group differences according to study hypotheses using linear models or pairwise comparisons with false-discovery-rate adjustment for multiplicity. For data on pre-post exposure changes, changes were first calculated at an individual animal level, and all analyses were conducted based on the pre-post exposure changes (Table 2). Statistical outliers were removed by performing a Grubbs Outlier Test ($p < 0.01$). Those removed data points were indicated in the specific table and figure legends.

3. Results

3.1. Laser Ablation and Bulk ICP-MS analyses confirmed W deposition and changes in elemental composition in the lungs

We used LA-ICP-MS imaging to confirm and characterize W particle distribution in sections from the left lobe of the lung (Fig. 2). W was clearly present in the lungs of exposed mice, despite being sampled 48 h after exposure. The intensity distribution appeared to be greater in the upper airways relative to the lower airways (Fig. 2, white arrows), although this was difficult to confirm at the level of resolution used for the LA-ICP-MS (50 μm spots). There was some evidence of W deposition making it into the lower airways. LA-ICP-MS also allowed examination of other elements in the lungs, which revealed several interesting observations. There was an increased intensity of iron throughout the lung sections in both AT-II treatment groups compared to the FA + Veh and W + Veh control groups. However, clear differences in intensity and distribution of copper in the lungs were difficult to define across the four groups based on the LA-ICP-MS images.

Because the laser ablation methods only provides relative quantifications, we conducted bulk ICP-MS on homogenates of the right caudal lung lobe. These data confirmed the significant deposition of W in exposed mice compared to the control groups ($p < 0.01$, $p < 0.001$) and there were no significant differences in tungsten deposition between the W + Veh and W + AT-II groups (Fig. 3A, Table 1). Bulk ICP-MS also confirmed that iron was elevated in the lungs of the AT-II treatment groups, but was only statistically significant in the W + AT-II group compared to the W + Veh group ($p < 0.001$). Iron levels were not altered by W exposure alone (Fig. 3B). Linear regression models indicated that the main effect was driven by AT-II treatment for iron (Table 1).

Interesting changes in trace metals zinc, magnesium, and molybdenum (Fig. 3C, D, H) were also observed in the lungs. W exposure (W + Veh and W + AT-II) decreased concentrations of essential metals zinc ($p < 0.01$, $p < 0.001$), magnesium ($p < 0.01$, $p < 0.001$), and molybdenum ($p < 0.001$) compared to the FA + Veh group. For molybdenum, the concentration in the lungs was further reduced in the W + AT-II group compared to the W + Veh group ($p < 0.05$). Linear regression models indicated that there were significant effects driven by both AT-II treatment and W exposure, but no interactive effect for zinc and molybdenum (Table 1). Copper levels decreased in the W + AT-II group compared to Veh control groups, which was not mirrored in the LA-ICP-MS images we acquired. Both W exposure and AT-II treatment and the combination (W + AT-II) also significantly reduced chromium concentrations in the lungs (Fig. 1 and Table 1). The Mean and SD for each metal analyzed is presented in Table 1 for each of the 4 experimental groups, including statistical analyses for effect mediation using linear regression analyses.

3.2. W particulate exposure and AT-II treatment alters cardiac function

Echocardiography assessment provided insights into changes in cardiac function between our experimental groups. Notably, a distinct response was observed in the groups exposed to W, where there was a significant decrease in both cardiac output and stroke volume following exposure (Fig. 4). AT-II treatment did not alter either cardiac output or stroke volume alone or in combination with W.

We also assessed tissue doppler motion of the LV free wall. The E' and A' indicators are critical parameters that provide information on LV free wall relaxation during the early and late phases of cardiac filling, respectively. Relative increases in A' indicate a shift towards greater late stage filling with a requirement of greater atrial contributions to LV filling. The W + AT-II group had a statistically significant elevation in the A'/E' ratio compared to W-Veh and a trending increase compared to the FA-AT-II group (Fig. 5). Neither AT-II nor W alone altered the A'/E' ratio compared to the FA-Veh group. Pre-post exposure changes Mean and SD for each cardiac outcome quantified by echocardiography are presented in Table 2.

Analysis of CTnI levels in the blood reveled a significant increase in levels in the W + AT-II group compared to the control groups (FA + Veh and W + Veh) and in the FA + AT-II group compared to the FA + Veh control group (Fig. 6). W exposure alone did not increase CTnI levels, consistent with the lack of increase in the A'/E' ratio after exposure. These findings provide further evidence to suggest that continuous administration of AT-II further drives cardiac injury following W exposure. In order to get a more mechanistic picture of the effects of W and AT-II on cardiac injury, a panel of cardiac remodeling and inflammation genes were profiled in left ventricle heart tissue using real-time qPCR. Despite evidence of altered cardiac function and increased levels of CTnl in the blood, there were no significant increases in any of the cardiac remodeling and inflammation genes, suggesting no evidence of increased cardiac remodeling or inflammation occurring in the heart following W exposure and/or AT-II treatment (Fig. 7).

3.3. Acute exposure to tungsten particles does not induce pulmonary inflammation in either experimental model

We have previously shown that inhalation exposure to W particles increases pulmonary inflammation in the BALF of female BALB/c mice (Templeton et al., 2023). In this study, total white blood cells, macrophages, and neutrophils were quantified in BALF to assess pulmonary inflammation. Cell differential analysis of BALF showed no statistically significant changes in the numbers of immune cells in the lungs among the different experimental groups, indicating that exposure to W and treatment with AT-II had no effect on pulmonary inflammation outcomes at the final terminal endpoint of the study (Fig. 8).

4. Discussion

In this study, we have demonstrated that acute inhalation exposure to W particles alone and in combination with continuous administration of AT-II leads to altered responses in cardiac function in male BALB/c mice. W exposure decreased cardiac output and stoke volume in both saline and AT-II-treated mice. Importantly these effects on cardiac function validate previous findings from our group demonstrating decreased cardiac output following acute exposure to W particles in

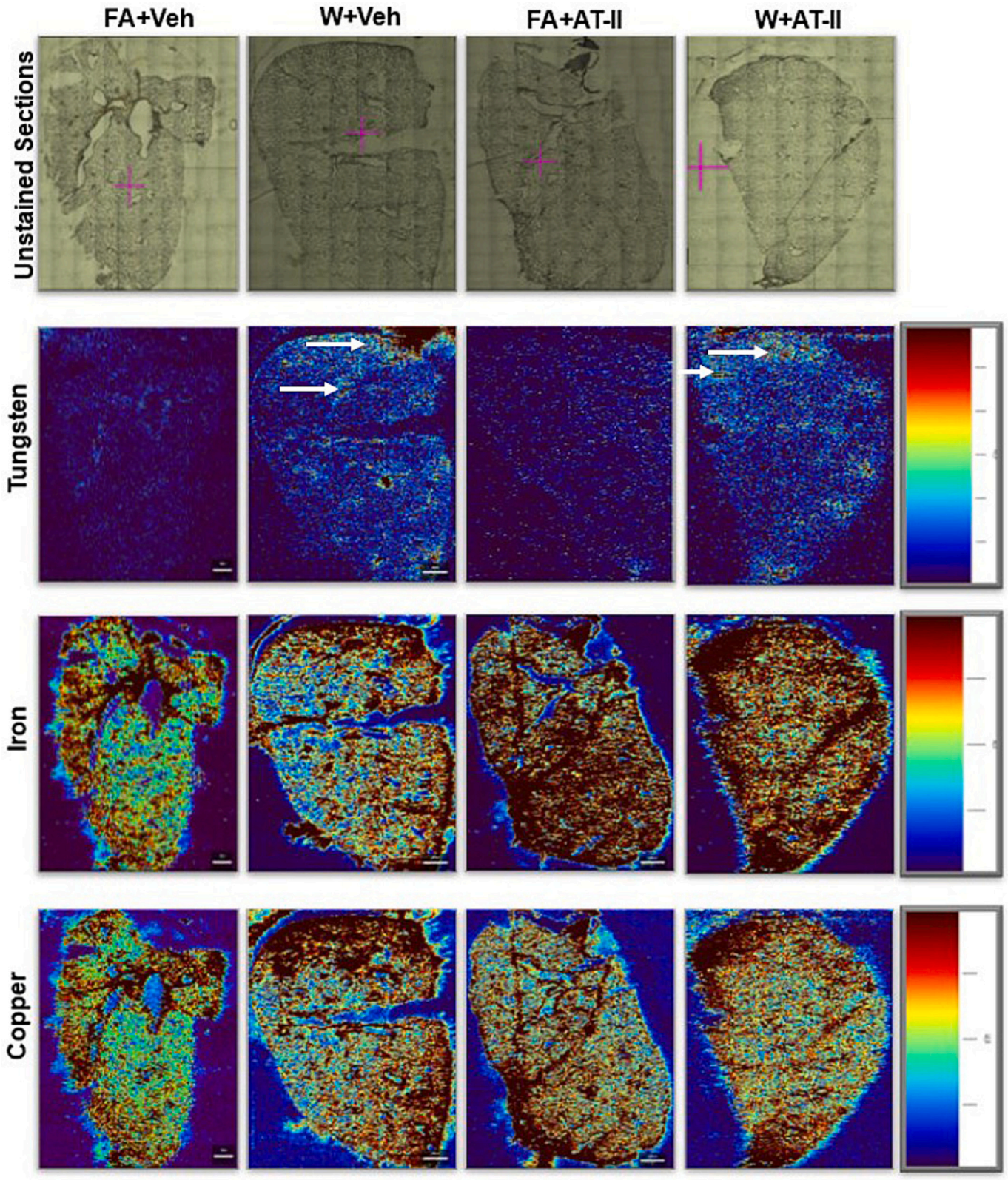

Fig. 2. Laser Ablation ICP-MS Analysis of metals in the lungs. Visual examination of element distributions illustrates the deposition of W particles in the exposure groups and also renders comparisons of iron and copper across all 4 experimental groups. Color scale indicates relative elemental concentration in tissue with dark red indicating the highest concentrated regions vs. dark blue indicating the lowest concentrated regions. Arrows show high concentrations of tungsten in the upper airway. Tissue sections were 20 μm in thickness. $n = 1$ per group. (For interpretation of the references to color in this figure legend, the reader is referred to the web version of this article.)

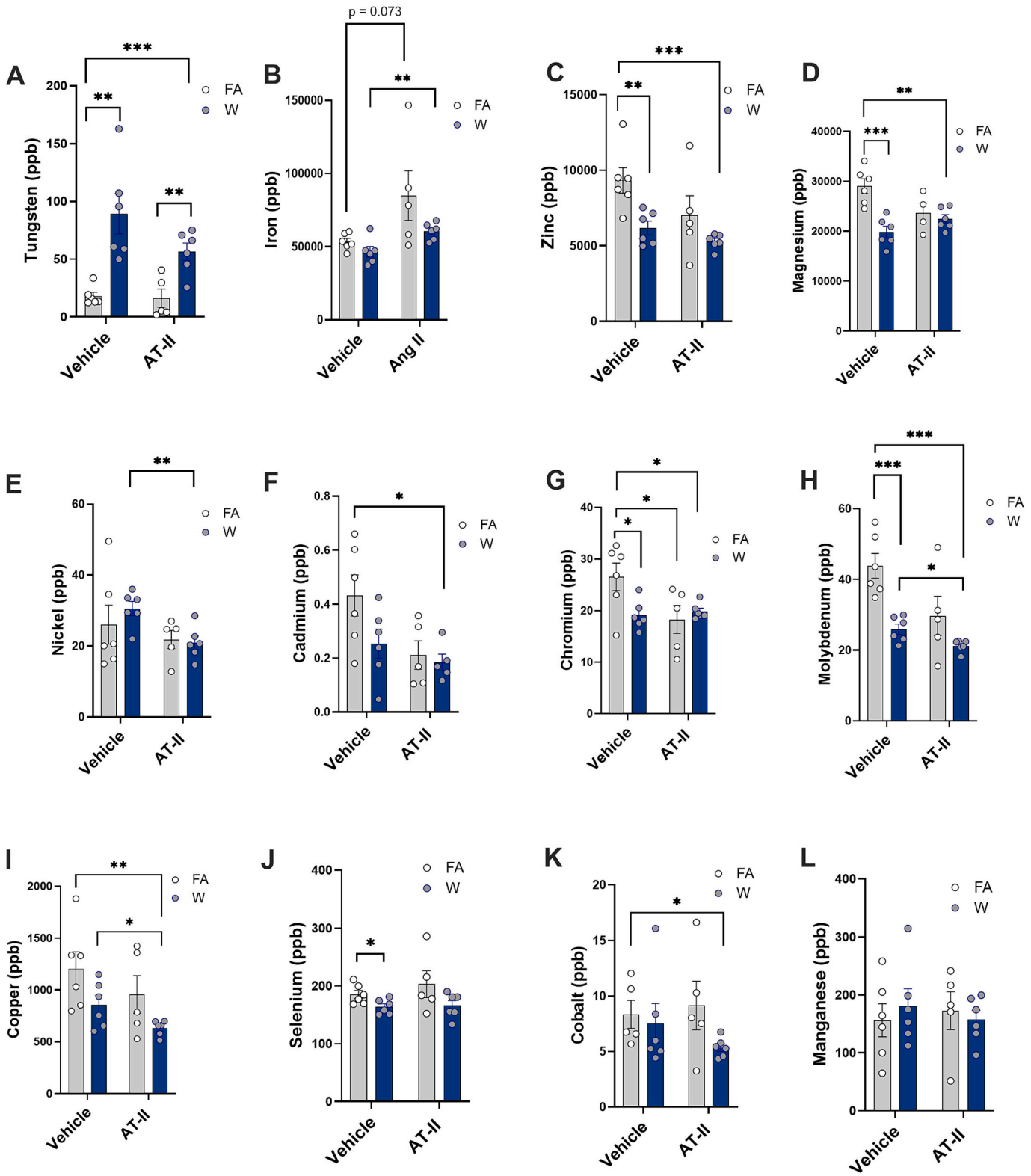

Fig. 3. Bulk ICP-MS elemental analysis of lung homogenates, normalized to tissue weights, reveals presence of W as a result of exposure, but also alteration of other metals due to either exposure, AT-II treatment, or both. Specific metals examined include W (A), iron (B), zinc (C), magnesium (D), nickel (E), cadmium (F), chromium (G), molybdenum (H), copper (I), selenium (J), cobalt (K), manganese (L). Asterisks denote significant difference between designated pairwise comparisons (*$p < 0.05$; **$p < 0.01$; ***$p < 0.001$). Outliers removed: magnesium – 1 in the FA + AT-II group, cobalt – 1 in the FA + Veh group, cadmium – 1 in the W + AT-II group.

Table 1
Elemental analyses of lungs by ICP-MS.

Group	FA + Veh		W + Veh		FA + AT-II		W + AT-II		
Parameters	Mean	SD	Mean	SD	Mean	SD	Mean	SD	p- value
Iron (Fe)	53,500	5628	46,629	8745	85,002	37,882	60,608	5794	0.01 (M)
Tungsten (W)	17.99	8.11	89.17	42.57	16.29	17.61	56.38	18.52	<0.001 (W)
Magnesium (Mg)	29,012	3593	19,817	2873	23,644	3854	22,457	2175	
Chromium (Cr)	26.53	6.53	19.12	2.85	18.27	6.11	19.83	1.52	0.009 (T) 0.013 (W) 0.033 (I)
Manganese (Mn)	156.17	69.88	181.19	72.11	172.63	73.15	157.29	39.57	
Cobalt (Co)	8.34	2.81	7.53	4.41	9.14	4.90	5.36	0.87	
Nickel (Ni)	26.04	13.47	30.57	4.94	21.84	5.70	20.89	4.62	
Copper (Cu)	1204	402	856	221	955	409	633	72	
Zinc (Zn)	9333	2071	6185	1105	7018	2911	5280	503	0.05 (T) 0.007 (W)
Selenium (Se)	185.23	17.15	164.15	12.66	203.05	51.47	166.11	21.54	
Molybdenum (Mo)	43.84	8.59	25.95	3.58	29.67	12.40	21.23	1.68	0.006 (T) <0.001 (W)
Cadmium (Cd)	0.43	0.19	0.25	0.13	0.21	0.12	0.18	0.07	

*Elemental concentrations in ppb; ng/g tissue weight. SD = standard deviation. *p*-values based on linear regression models. *Only p-values <0.05 are reported. W: main effect exposure; T: main effect of treatment, I: interaction. Outliers removed: magnesium – 1 in the FA + AT-II group, cobalt – 1 in the FA + Veh group, cadmium – 1 in the W + AT-II group.

female BALB/c mice (Templeton et al., 2023). However, treatment with AT-II did not further exacerbate the effects of W exposure on these cardiac outcomes.

The A'/E' or E'/A' ratio is a key measurement for assessing diastolic function by comparing early (E') and late (A') diastolic filling velocities of the left ventricle (Mottram and Marwick, 2005). During diastole, the ventricles relax and fill with blood. The E' wave signifies early filling, driven by blood flowing from the left atrium when the atrioventricular (AV) valves open. In contrast, the A' wave corresponds to late filling when the atria contracts to propel more blood into the ventricle (Ancona et al., 2014; Chaves et al., 2001; Hanton et al., 2008; Mao et al., 2019; Naredo and Monteagudo, 2014; Pellett and Kerut, 2004; Villalba-Orero et al., 2022). In this study, the A'/E' ratio was significantly increased in the W + AT-II group compared to the W + Veh group and trending increase compared to the FA + AT-II group. This was observed at a concentration of AT-II that is approximately 50% lower than published studies in BALB/c mice that led to hypertension and cardiac remodeling (Peng et al., 2011). This would suggest that the atria in the W + AT-II group of mice had to exert significantly greater effort to fill the heart effectively.

Such an observation could be indicative of heightened atrial stress and increased resistance encountered during the filling phase and could indicate diastolic dysfunction in the W + AT-II group, which may be linked to conditions such as ventricular hypertrophy or stiffening of the heart muscle. In some cases, severely decreased A'/E' ratios can indicate severe aortic regurgitation or constrictive pericarditis. Importantly, W exposure alone did not lead to an increase in the A'/E' ratio. This is not consistent with our previous study where we did observe a significance increase in A' following W exposure in female BALB/c mice (Templeton et al., 2023), suggesting that female mice might be more sensitive than male mice to tungsten-mediated diastolic dysfunction.

CTnI is primarily produced in the myocardium. When cardiomyocytes are damaged, such as during myocardial infarction (heart attack), CTnI is released into the bloodstream serving as a biomarker that indicates heart muscle damage (Babuin and Jaffe, 2006; Potter et al., 2022). The amount of CTnI released into the bloodstream is proportional to the extent of heart muscle damage. We found that CTnI increased in the W + AT-II group compared to the control groups (FA + Veh and W + Veh). This suggests that AT-II treatment interacts with W exposure to induce cardiac injury in this model.

Our data suggests that there may be multiple mechanisms driving altered cardiac function and cardiac injury following W exposure, both AT-II dependent and AT-II independent mechanisms. Based on our gene expression analyses of heart tissue, this early acute timepoint was not long enough to see changes in cardiac remodeling genes or inflammation genes in the heart following exposure to W and/or treatment with AT-II despite observing changes in cardiac function. Future work will focus on performing staining of heart tissue following chronic W and W + AT-II treatment to look at markers of damage including levels of collagen, smooth muscle actin, and fibronectin. In addition, we will also explore molecular drivers of these changes in cardiac function and injury and dissect out the role AT-II plays in the process and any sex-specific differences in response.

In our previous study, performed in female BALB/c mice, acute inhalation of W particulates resulted in W accumulation in the lungs, but not the heart following acute exposure (Templeton et al., 2023). This suggests that the alterations in cardiac function were driven by secondary mediators from the lungs, not direct effects on the heart. In our previous study, we found that inhalation to W particles resulted in a sustained increase in mild pulmonary inflammation in the lungs, characterized by an increase in the number of macrophages (Templeton et al., 2023), suggesting that inflammatory mediators could be driving the effects observed in the heart. In contrast, the analysis of BALF in the current study did not show any significant alterations in the number of white blood cells or the number of macrophages or neutrophils in the lungs, suggesting no sustained pulmonary inflammation. However, a more sequential time course of changes in pulmonary inflammation following exposure should be performed to determine if this is due to no induction in inflammation or increased resolution of inflammation in the male mice. This discrepancy may be attributed to differences in sex between the two studies. Other studies have demonstrated that inflammatory processes in the lungs can be different between sexes

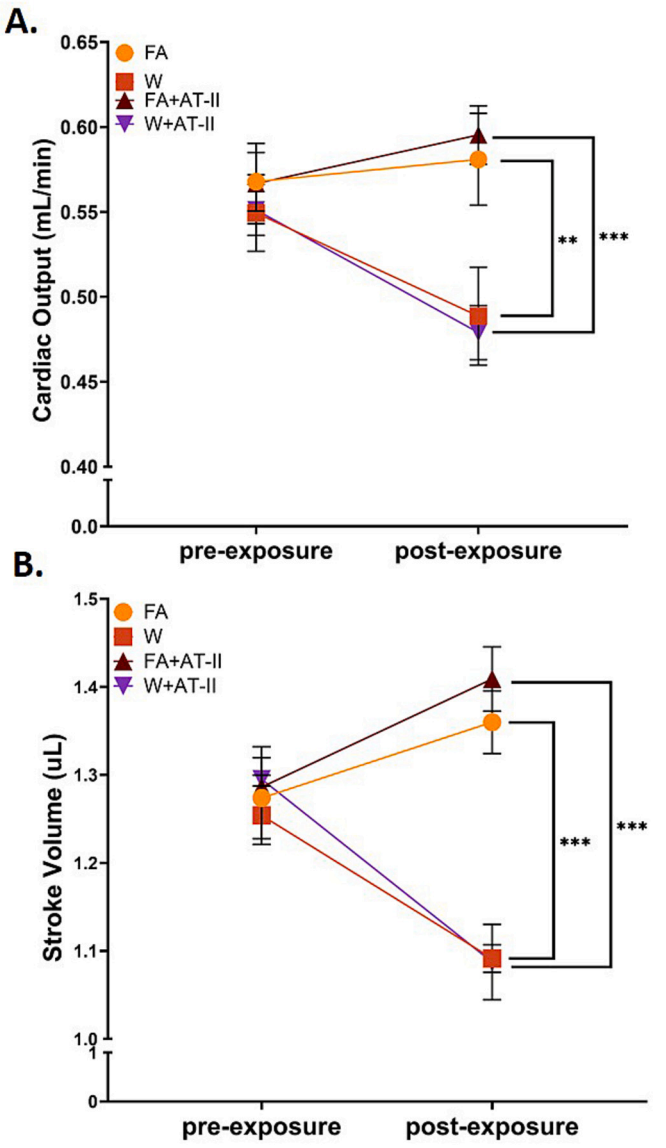

Fig. 4. Echocardiographic data obtained prior to exposures and after the final exposure to W. Cardiac output (A), stroke volume (B) were normalized to the body weight of mice at the time of measurement. Asterisks denote significant difference between designated pre-post exposure changes pairwise comparisons (**$p < 0.01$; ***$p < 0.001$).

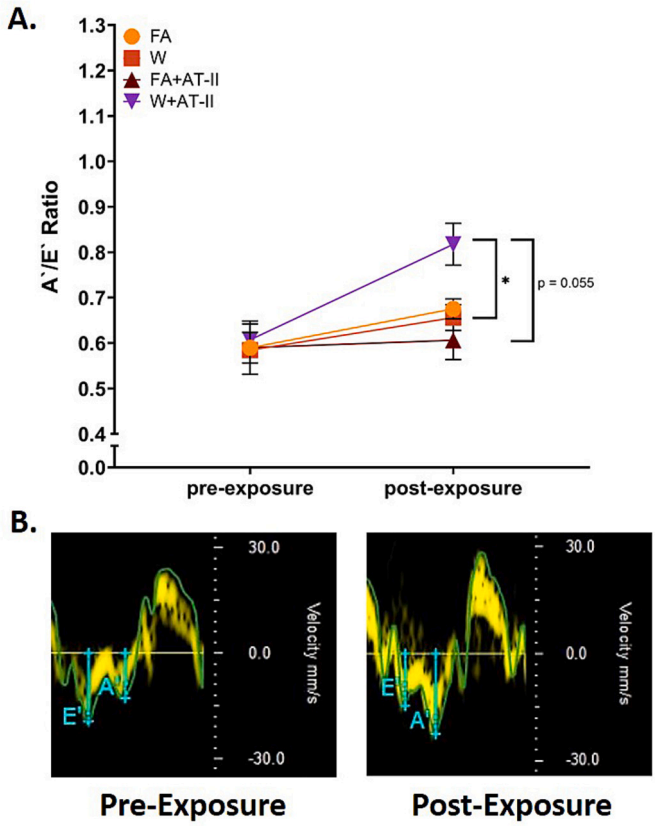

Fig. 5. A. Inhaled W particle exposure precipitated early diastolic dysfunction in the heart. The ratio of late ventricular filling (A′) to early ventricular filling (E′) representing diastolic function (A′/E′ ratio), was determined from tissue doppler motion of the LV free wall. B. Examples of LV free wall tissue doppler traces for pre-exposure and post-exposure in the W + AT-II group. Asterisk denotes significant difference between designated pre-post exposure changes pairwise comparisons (*$p < 0.05$). Outlier removed: Post-exposure - 1 in the FA + Veh group.

following inhalation exposure to toxicants, including altered timing of when the inflammation occurs (Cabello et al., 2015; Shvedova et al., 2015; Yaeger et al., 2021). Comparing the two studies also indicates differences in tungsten-mediated cardiac injury and altered function, where female mice were more sensitive to tungsten-mediated diastolic dysfunction than male mice, which could be driven by inflammatory mediators. Future work will need to dissect out what role pulmonary inflammation plays in the altered cardiac function and tissue damage driven by W exposure and any sex-specific differences in these mediators. In addition, there were differences in tungsten deposition in the lungs between these two studies. The mean tungsten deposition in the lungs of the W-exposed animals was lower in the male mice than in our previously published study in female mice (72.78 ppb ± 35.68 SD vs. 203.50 ppb ± 35.92 SD). It will also be important to determine if this differential tungsten deposition in the lungs contributed to these sex-specific differences in the lungs and the heart following W inhalation exposure.

A new piece of information gained from this study was the additional elemental changes in the lungs following inhalation exposure to W and/or treatment with AT-II. The LA-ICP-MS images showed deposition of tungsten predominantly in the upper airway of the lungs, which could be due to initial deposition or accumulation due to mucociliary clearance. However, there was evidence of some W deposition in the lower airway, suggesting some particles do penetrate into the deep lung. Our LA-ICP-MS and bulk ICP-MS studies also showed that there was an increase in the amount of iron in the lungs in the AT-II treatment groups (FA + AT-II and W + AT-II). Previous studies have reported iron deposition in cells and tissues following AT-II administration (Ishizaka et al., 2002; Ishizaka et al., 2005). This could be an indirect measure of AT-II treatment in this model. One explanation for this increase in iron is that AT-II treatment can increase iron transporters Transferrin receptor (TfR), divalent metal transporter (DMT1), and DMT1, Ferroportin 1 (FPN) in the kidneys and small intestines (Ishizaka et al., 2007; Tajima et al., 2015). Iron is an essential mineral for various physiological processes in the body, including oxygen transport, energy production, and immune function and imbalances can impact lung health (National Institutes of Health, n.d.-a; Wessling-Resnick, 2017). Conditions like hemochromatosis can cause excessive iron, harming lung tissues and potentially leading to diseases like fibrosis (Porter and Rawla, n.d.). High iron levels can also generate harmful molecules of reactive oxygen species, causing oxidative stress which could be linked to lung diseases like Chronic Obstructive Pulmonary Disease and cancer (Boukhenouna et al., 2018). In addition, some bacteria and pathogens require iron for their growth and survival, elevated iron can promote pathogen growth, increasing

Table 2
Pre-post changes in echocardiography outcomes.

Parameters	FA + Veh		W + Veh		FA + AT-II		W + AT-II		p- value
	Mean	SD	Mean	SD	Mean	SD	Mean	SD	
Diameter,s	0.043	0.337	−0.0188	0.429	0.016	0.511	−0.0178	0.479	ns
Diameter,d	0.086	0.246	−0.233	0.328	0.074	0.3842	−0.254	0.384	ns
Volume,s	−0.070	0.422	−0.361	0.569	−0.098	0.604	−0.377	0.575	ns
Volume,d	−0.096	0.441	−0.622	0.605	−0.086	0.531	−0.702	0.617	ns
LVAW,s	0.230	0.164	0.196	0.167	0.020	0.226	0.181	0.179	ns
LVAW,d	0.187	0.170	0.203	0.194	−0.003	0.246	0.190	0.193	ns
LVPW,s	0.089	0.204	0.247	0.297	0.045	0.443	−0.072	0.227	ns
LVPW,d	0.085	0.138	0.243	0.263	0.025	0.340	0.023	0.144	ns
LV mass	30.12	16.69	30.68	30.70	7.58	50.00	9.19	27.97	ns
LV mass Cor	24.10	13.35	24.54	24.56	6.06	40.00	7.35	22.38	ns
Ejection Fraction	0.89	6.37	0.41	8.19	1.65	11.37	−0.75	8.81	ns
Fractional Shortening	0.64	3.76	0.16	4.60	0.92	6.75	−0.53	5.04	ns
Cardiac Output	0.013	0.032	−0.061	0.037	0.029	0.032	−0.072	0.022	a**, c**
Stroke Volume	0.086	0.052	−0.163	0.081	0.123	0.096	−0.208	0.120	a***,c***
A`/E`	0.081	0.093	0.072	0.088	0.032	0.140	0.210	0.112	c $p = 0.055$, d*

*Significant in: Comparing Pre-post Change FA + Veh vs. W + Veh: a; FA + Veh vs. FA + AT-II: b; FA + AT-II vs W + AT-II: c; W + Veh vs. W + AT-II: d; not significant: ns.
Abbreviations: LV: Left ventricle; s: systolic; d: diastolic; AW: anterior wall; PW: posterior wall; E`: early diastolic tissue velocity; A`: late diastolic tissue velocity. Corrected p-value * $p < 0.05$; ** $p < 0.01$, *** $p < 0.001$. Outlier removed: Post-exposure - 1 in the FA + Veh group.

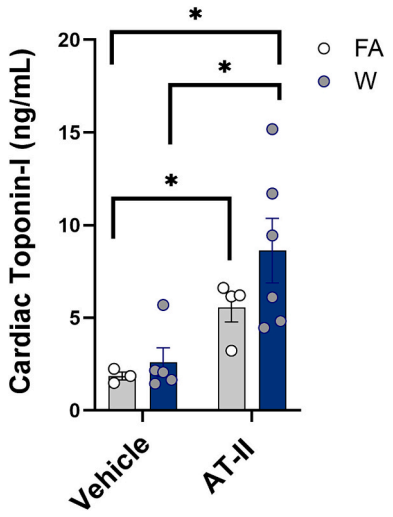

Fig. 6. CTnI concentrations in blood samples assessed by an iStat point-of-care device. Asterisks denote significant difference between designated pairwise comparisons (*$p < 0.05$).

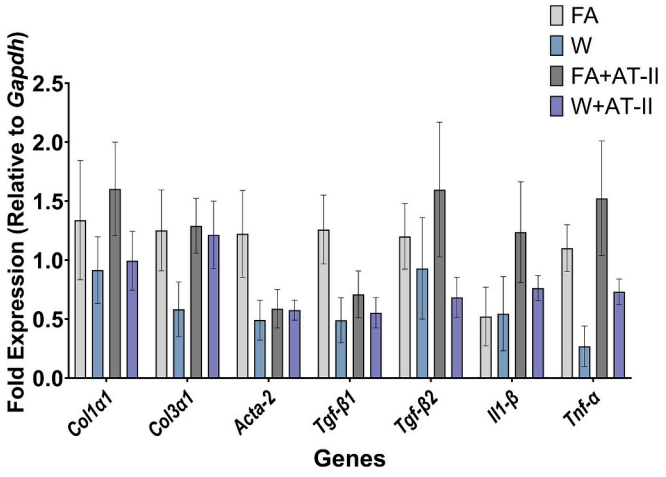

Fig. 7. Gene expression of cardiac remodeling and inflammation genes was quantified in left ventricle heart tissue by real-time qPCR. Data express the mean fold change ± SD relative to the housekeeping gene *Gapdh*.

lung infection susceptibility (Cherayil, 2011).

In addition, our data showed reduced levels of zinc, magnesium, and molybdenum in the W-exposed groups compared to the FA + Veh control group. Zinc plays a crucial role in various physiological processes in the human body, including immune function, wound healing, and cell growth and also has enzyme activity as a cofactor in metalloenzymes and metalloproteins (National Institutes of Health, n.d.-b). Zinc possesses anti-inflammatory, antioxidant, immune, and metabolic modulatory properties in the lungs (Jarosz et al., 2017). Deficiency in zinc can weaken the immune response, making individuals more susceptible to respiratory infections such as pneumonia and bronchitis. Zinc is also involved in wound healing and tissue repair. Deficiency in zinc can lead to delayed wound healing in the lungs, potentially affecting recovery from lung injuries or infections (Lin et al., 2017). Magnesium deficiency can enhance the action of calcium, leading to increased bronchial smooth-muscle contraction and greater sensitivity of the airways, which can heightened reactivity and may result in asthma-like symptoms, including wheezing and shortness of breath (Landon and Young, 1993). Low magnesium levels could impact the muscles controlling breathing, potentially reducing lung function, capacity, and respiratory efficiency (Amaral et al., 2012). Molybdenum is an essential trace element integral to the active sites of over fifty enzymes involved in diverse redox reactions and oxygen atom transfer. Molybdenum is an essential element required by enzymes that catalyze key reactions in the carbon, sulfur and nitrogen metabolism, underscoring the indispensable nature of molybdenum in various physiological processes (Mendel and Bittner, 2006; He et al., 2022). Deficiency in molybdenum cofactors can lead to severe inborn errors of metabolism, often resulting in early childhood mortality. There is also a strong association between excessive molybdenum and pulmonary tissue damage, such as pulmonary fibrosis, pneumonia, and even lung cancer (Bai et al., 2020). W can displace molybdenum in many molybdenum requiring enzymes, leading to reduced enzyme activity (Schröder et al., 2006). It would be interesting to determine the mechanism leading to decreased molybdenum concentrations in the lungs following W exposure and what function this plays in W-mediated toxicity in the lungs and heart in future studies. In addition, utilization of metabolomics in future studies may unveil further insights into if and how these elemental changes contribute to disease pathologies in this model following W exposure.

The concentration of W particles used in our study reflects levels

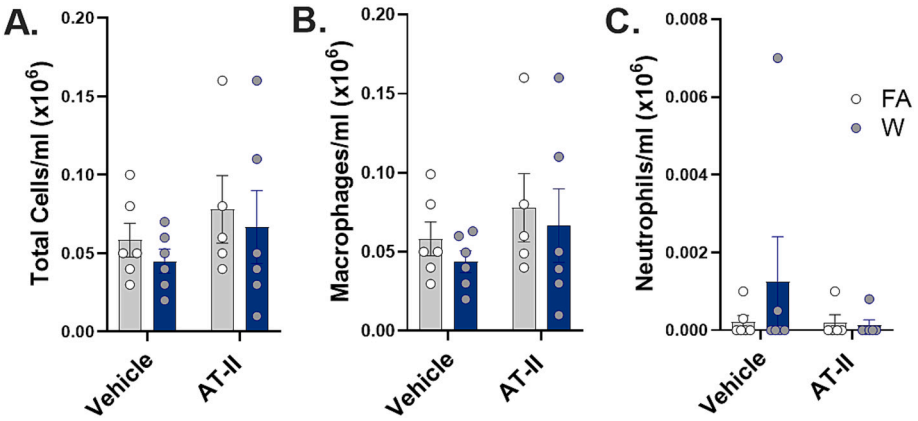

Fig. 8. Differential immune cell analysis was conducted on BALF after exposure to inhaled W particles. The figure presents data on the total number of white blood cells (A), macrophages (B), and polymorphonuclear neutrophils (C) in BALF.

commonly found in occupational settings such as hard metal manufacturing and military environments (Kraus et al., 2001). We opted for a whole-body exposure system due to our previous research on the effects of inhaled W using this apparatus (Miller et al., 2021; Templeton et al., 2023). This system simulates inhalation exposure by generating a continuous flow of aerosolized particles to freely moving mice within their cages. This approach minimizes stress on the mice and emulates conditions akin to human inhalation exposure scenarios.

In summary, these findings collectively emphasize the intricate relationships between W exposure and AT-II treatment contributing to cardiac injury and altered cardiac function. This work also highlights the importance of considering elemental homeostasis and its potential implications for health and disease. Further exploration into these interactions, in addition to interactions between sex and stain of mice could yield valuable insights into the underlying mechanisms driving tungsten-altered cardiac function and the development of cardiovascular disease.

CRediT authorship contribution statement

Milad MazloumiBakhshayesh: Writing – review & editing, Writing – original draft, Visualization, Methodology, Investigation, Formal analysis. **Russell P. Hunter:** Writing – review & editing, Writing – original draft, Methodology, Investigation, Formal analysis. **Brenna Baird:** Investigation. **Rui Liu:** Investigation, Formal analysis. **Anahi Gabriela Jimenez-Campos:** Investigation. **Siem Goitom:** Investigation. **Edward B. Barr:** Methodology, Investigation, Formal analysis. **Guy W. Herbert:** Investigation, Formal analysis. **Selita N. Lucas:** Investigation. **Charlotte M. McVeigh:** Visualization, Formal analysis. **Jorge Moreno:** Visualization, Formal analysis. **Yiliang Zhu:** Writing – review & editing, Visualization, Funding acquisition, Formal analysis. **Barry E. Bleske:** Writing – review & editing, Writing – original draft, Methodology, Funding acquisition, Formal analysis, Conceptualization. **Matthew J. Campen:** Writing – review & editing, Writing – original draft, Visualization, Methodology, Investigation, Funding acquisition, Formal analysis, Conceptualization. **Alicia M. Bolt:** Writing – review & editing, Writing – original draft, Visualization, Methodology, Funding acquisition, Formal analysis, Conceptualization.

Declaration of competing interest

The authors declare no conflicts of interest with the content of this manuscript.

Acknowledgements

This study was funded in part by the National Institutes of Health grants (the National Institute of General Medical Sciences - P20GM130422; the National Institute of Environmental Health Sciences - R01ES014639, P42ES025589, P30ES032755; the Eunice Kennedy Shriver National Institute of Child Health and Human Development - F31HD107945; and the National Cancer Institute -P30CA118100) and the Centers of Disease Control and Prevention grant (National Insitute for Occupational Safety and Health - 1R21OH012552).

Appendix A. Supplementary data

Supplementary data to this article can be found online at https://doi.org/10.1016/j.taap.2026.117753.

Data availability

Data will be publicly available through an open access digital repository immediately following publication acceptance.

References

Agarwal, S., Zaman, T., Tuzcu, E.M., Kapadia, S.R., 2011. Heavy metals and cardiovascular disease: results from the National Health and nutrition examination survey (NHANES) 1999-2006. Angiology 62 (5), 422–429.

Agency for Toxic Substances and Disease Registry, A, 2005. Toxicological profile for tungsten. Online Access. www.atsdr.cdc.gov/toxprofiles/tp186.pdf. Last Accessed: September 1st, 2025.

Almoshari, Y., 2022. Osmotic pump drug delivery systems-a comprehensive review. Pharmaceuticals (Basel) 15 (11), 1430. Nov 18.

Amaral, A.F., Gallo Jr., L., Vannucchi, H., Crescêncio, J.C., Vianna, E.O., Martinez, J.A., 2012. The effect of acute magnesium loading on the maximal exercise performance of stable chronic obstructive pulmonary disease patients. Clinics (Sao Paulo) 67 (6), 615–622.

Ancona, R., Comenale Pinto, S., Caso, P., D'Andrea, A., Di Salvo, G., Arenga, F., Coppola, M.G., Sellitto, V., Macrino, M., Calabrò, R., 2014. Left atrium by echocardiography in clinical practice: from conventional methods to new echocardiographic techniques. ScientificWorldJournal 2014, 451042.

Azevedo, P.S., Polegato, B.F., Minicucci, M.F., Paiva, S.A., Zornoff, L.A., 2016. Cardiac remodeling: concepts, clinical impact, pathophysiological mechanisms and pharmacologic treatment. Arq. Bras. Cardiol. 106 (1), 62–69.

Babuin, L., Jaffe, A.S., 2006. Troponin: the biomarker of choice for the detection of cardiac injury. CMAJ, 2005. 173(10):1191–202. Erratum in: CMAJ, 2005. 173(12): 1490. Erratum in: CMAJ 174 (3), 353.

Bai, Y., Wang, G., Fu, W., Lu, Y., Wei, W., Chen, W., Wu, X., Meng, H., Feng, Y., Liu, Y., Li, G., Wang, S., Wang, K., Dai, J., Li, H., Li, M., Huang, J., Li, Y., Wei, S., Yuan, J., Yao, P., Miao, X., He, M., Zhang, X., Yang, H., Wu, T., Guo, H., 2020. Circulating essential metals and lung cancer: Risk assessment and potential molecular effects. Environ Int, 2019. 127:685-693. Erratum in: Environ Int 143, 106072.

Bolt, A.M., Mann, K.K., 2016. Tungsten: an emerging toxicant, alone or in combination. Curr. Environ. Health Rep 3, 405–415.

Boukhenouna, S., Wilson, M.A., Bahmed, K., Kosmider, B., 2018. Reactive oxygen species in chronic obstructive pulmonary disease. Oxid. Med. Cell. Longev. 2018, 5730395.

Cabello, N., Mishra, V., Sinha, U., DiAngelo, S.L., Chroneos, Z.C., Ekpa, N.A., Cooper, T. K., Caruso, C.R., Silveyra, P., 2015. Sex differences in the expression of lung inflammatory mediators in response to ozone. Am. J. Physiol. Lung Cell. Mol. Physiol. 309 (10), L1150–L1163.

CDC, 2003. Second national report on human exposure to environmental chemicals. Online Access. https://www.cdc.gov/environmental-exposure-report/ (Last Accessed December 10th, 2025).
Chaves, A.A., Weinstein, D.M., Bauer, J.A., 2001. Non-invasive echocardiographic studies in mice: influence of anesthetic regimen. Life Sci. 69 (2), 213–222.
Cherayil, B.J., 2011. The role of iron in the immune response to bacterial infection. Immunol. Res. 50 (1), 1–9.
Cohn, J.N., Ferrari, R., Sharpe, N., 2000. Cardiac remodeling–concepts and clinical implications: a consensus paper from an international forum on cardiac remodeling. Behalf of an International Forum on Cardiac Remodeling. J Am Coll Cardiol 35 (3), 569–582.
Colombo, E.S., Davis, J., Makvandi, M., et al., 2013. Effects of nicotine on cardiovascular remodeling in a mouse model of systemic hypertension. Cardiovasc. Toxicol. 13, 364–369.
Dams, R., Robbins, J.A., Rahn, K.A., Winchester, J.W., 1970. Nondestructive neutron activation analysis of air pollution particulates. Anal. Chem. 42, 861–867.
Day, G.A., Stefaniak, A.B., Virji, M.A., 2009. Characterization of Exposures Among Cemented Tungsten Carbide Workers. Part I: Size-Fractionated Exposures to Airborne Cobalt and Tungsten. Online Access. https://stacks.cdc.gov/view/cdc/187228.
Dries, J.L., Kent, S.D., Virag, J.A., 2011. Intramyocardial administration of chimeric ephrinA1-fc promotes tissue salvage following myocardial infarction in mice. J. Physiol. 589 (Pt 7), 1725–1740.
Fuchs, F.D., Whelton, P.K., 2020. High blood pressure and cardiovascular disease. Hypertension 75 (2), 285–292.
Gaitens, J.M., Condon, M., Squibb, K.S., Centeno, J.A., McDiarmid, M.A., 2017. Metal exposure in veterans with embedded fragments from war-related injuries: early findings from surveillance efforts. J. Occup. Environ. Med. 59 (11), 1056–1062.
Gonzalez-Villalobos, R.A., Seth, D.M., Satou, R., Horton, H., Ohashi, N., Miyata, K., Katsurada, A., Tran, D.V., Kobori, H., Navar, L.G., 2008. Intrarenal angiotensin II and angiotensinogen augmentation in chronic angiotensin II-infused mice. Am. J. Physiol. Renal Physiol. 295 (3), F772–F779.
Haddad, E., Zikovsky, L., 1985. Determination of Al, as, Cr, Cs, Fe, Mn, Sb, Sc, W and Zn in the workroom air by instrumental neutron activation analysis. J. Radioanal. Nucl. Chem. 93 (6), 371–378.
Hanton, G., Eder, V., Rochefort, G., Bonnet, P., Hyvelin, J.M., 2008. Echocardiography, a non-invasive method for the assessment of cardiac function and morphology in preclinical drug toxicology and safety pharmacology. Expert Opin. Drug Metab. Toxicol. 4 (6), 681–696.
Hartley, C.J., Reddy, A.K., Madala, S., Michael, L.H., Entman, M.L., Taffet, G.E., 2008. Doppler estimation of reduced coronary flow reserve in mice with pressure overload cardiac hypertrophy. Ultrasound Med. Biol. 34 (6), 892–901.
He, X.T., Li, X., Zhang, M., Tian, B.M., Sun, L.J., Bi, C.S., Deng, D.K., Zhou, H., Qu, H.L., Wu, C., Chen, F.M., 2022. Role of molybdenum in material immunomodulation and periodontal wound healing: targeting immunometabolism and mitochondrial function for macrophage modulation. Biomaterials 283, 121439.
Health Canada, 2013. Second report on human biomonitoring of environmental chemicals in Canada. Available at: https://www.canada.ca/en/health-canada/services/environmental-workplace-health/reports-publications/environmental-contaminants/second-report-human-biomonitoring-environmental-chemicals-canada-health-canada-2013.html. Last Accessed December 10th, 2025.
Ishizaka, N., Aizawa, T., Yamazaki, I., et al., 2002. Abnormal Iron deposition in renal cells in the rat with chronic angiotensin II administration. Lab. Invest. 82, 87–96.
Ishizaka, N., Saito, K., Noiri, E., Sata, M., Ikeda, H., Ohno, A., Ando, J., Mori, I., Ohno, M., Nagai, R., 2005. Administration of ANG II induces iron deposistion and upregulation of TGF-β1 mRNA in the rat liver. Am. J. Phys. Regul. Integr. Comp. Phys. 288 (4), R1063–R1070.
Ishizaka, N., Saito, K., Furuta, K., Matsuzaki, G., Koike, K., Noiri, E., Nagai, R., 2007. Angiotensin II-induced regulation of the expression and localization of iron metabolism-related genes in the rat kidney. Hypertens. Res. 30 (2), 195–202.
Jagielak, J., Mamont-Ciesla, K., 1979. Relationships among concentrations of airborne metals in industrial districts. J. Radioanal. Chem. 52 (2), 461–470.
Jarosz, M., Olbert, M., Wyszogrodzka, G., Młyniec, K., Librowski, T., 2017. Antioxidant and anti-inflammatory effects of zinc. Zinc-dependent NF-κB signaling. Inflammopharmacology 25 (1), 11–24.
Keith, L.S., Wohlers, D.W., Moffett, D.B., Rosemond, Z.A., 2007. Agency for Toxic Substances and Disease Registry. ATSDR evaluation of potential for human exposure to tungsten. Toxicol. Ind. Health 23, 309–345.
Klasson, M., Bryngelsson, I.L., Pettersson, C., Husby, B., Arvidsson, H., Westberg, H., 2016. Occupational exposure to cobalt and tungsten in the Swedish hard metal industry: air concentrations of particle mass, number, and surface area. Ann. Occup. Hyg. 60 (6), 684–699.
Kraus, T., Schramel, P., Schaller, K.H., Zöbelein, P., Weber, A., Angerer, J., 2001. Exposure assessment in the hard metal manufacturing industry with special regard to tungsten and its compounds. Occup. Environ. Med. 58 (10), 631–634.
Landon, R.A., Young, E.A., 1993. Role of magnesium in regulation of lung function. J. Am. Diet. Assoc. 93 (6), 674–677.
Lasfargues, G., Lison, D., Maldague, P., Lauwerys, R., 1992. Comparative study of the acute lung toxicity of pure cobalt powder and cobalt tungsten carbide mixture in rat. Toxicol and Appl Pharm 112, 41–50.
Lasfargues, G., Lardot, C., Delos, M., Lauwerys, R., Lison, D., 1995. The delayed lung responses to single and repeated intratracheal administration of pure cobalt and hard metal powder in the rat. Environ Research 69, 108–121.
Lin, P.H., Sermersheim, M., Li, H., Lee, P.H.U., Steinberg, S.M., Ma, J., 2017. Zinc in wound healing modulation. Nutrients 10 (1), 16.
Machado, B.I., Murr, L.E., Suro, R.M., Gaytan, S.M., Ramirez, D.A., Garza, K.M., Schuster, B.E., 2010. Characterization and cytotoxic assessment of ballistic aerosol particulates for tungsten alloy penetrators into steel target plates. Int. J. Environ. Res. Public Health 7 (9), 3313–3331.
Mao, Y.K., Zhao, B.W., Zhou, L., Wang, B., Chen, R., Wang, S.S., 2019. Z-score reference ranges for pulsed-wave Doppler indices of the cardiac outflow tracts in normal fetuses. Int. J. Cardiovasc. Imaging 35 (5), 811–825.
McKernan, J.L., Toraason, M.A., Fernback, J.E., Petersen, M.R., 2009 Apr. Presence of tungsten-containing fibers in tungsten refining and manufacturing processes. Ann. Occup. Hyg. 53 (3), 215–224.
Mendel, R.R., Bittner, F., 2006. Cell biology of molybdenum. Biochim Biophys Acta - Mol Cell Res 1763 (7), 621–635.
Miller, K., McVeigh, C.M., Barr, E.B., Herbert, G.W., Jacquez, Q., Hunter, R., Medina, S., Lucas, S.N., Ali, A.S., Campen, M.J., Bolt, A.M., 2021. Inhalation of tungsten metal particulates alters the lung and bone microenvironments following acute exposure. Toxicol. Sci. 184 (2), 286–299.
Mills, K.T., Stefanescu, A., He, J., 2020. The global epidemiology of hypertension. Nat. Rev. Nephrol. 16 (4), 223–237.
Mottram, P.M., Marwick, T.H., 2005. Assessment of diastolic function: what the general cardiologist needs to know. Heart 91 (5), 681–695.
Naredo, E., Monteagudo, I., 2014. Doppler techniques. Clin. Exp. Rheumatol. 32 (1 Suppl 80), S12–S19.
National Institutes of Health. Iron, Fact Sheet for Health Professionals. Online Access. https://ods.od.nih.gov/factsheets/Iron-HealthProfessional/. Last Accessed: September 1st 2025.
National Institutes of Health. Zinc, Fact Sheet for Health Professionals. Online Access. https://ods.od.nih.gov/factsheets/Zinc-HealthProfessional/. Last Accessed: September 1st 2025.
Nigra, A.E., Howard, B.V., Umans, J.G., Best, L., Francesconi, K.A., Goessler, W., Devereux, R., Navas-Acien, A., 2018. Urinary tungsten and incident cardiovascular disease in the strong heart study: an interaction with urinary molybdenum. Environ. Res. 166, 444–451.
Paschal, D.C., Ting, B.G., Morrow, J.C., Pirkle, J.L., Jackson, R.J., Sampson, E.J., Miller, D.T., Caldwell, K.L., 1998. Trace metals in urine of United States residents: reference range concentrations. Environ. Res. 76, 53–59.
Pellett, A.A., Kerut, E.K., 2004. The Doppler equation. Echocardiography 21 (2), 197–198.
Peng, H., Yang, X.P., Carretero, O.A., Nakagawa, P., D'Ambrosio, M., Leung, P., Xu, J., Peterson, E.L., González, G.E., Harding, P., Rhaleb, N.E., 2011 Aug. Angiotensin II-induced dilated cardiomyopathy in Balb/c but not C57BL/6J mice. Exp Physiol 96 (8), 756–764. https://doi.org/10.1113/expphysiol.2011.057612. Epub 2011 May 20. PMID: 21602297; PMCID: PMC3256574.
Porter, J.L., Rawla, P.. Hemochromatosis. National Library of Medicine. Online Access. https://www.ncbi.nlm.nih.gov/books/NBK430862/.
Potter, J.M., Hickman, P.E., Cullen, L., 2022. Troponins in myocardial infarction and injury. Aust. Prescr. 45 (2), 53–57.
Prajapati, M.V., Adebolu, O.O., Marrow, B.M., Cerreta, J.M., 2017. Evaluation of pulmonary response to inhaled tungsten (IV) oxide nanoparticles in golden Syrian hamsters. Exp Biol and Med 242, 29–44.
Rajendran, N., Hu, S.C., Sullivan, D., Muzzio, M., Detrisac, C.J., Venezia, C., 2012. Toxicologic evaluation of tungsten: 28-day inhalation study of tungsten blue oxide in rats. Inhal. Toxicol. 24 (14), 985–994.
Rengasamy, A., Kommineni, C., Jones, J.A., Fedan, J.S., 1999. Effects of hard metal on nitric oxide pathways and airway reactivity to methacholine in rat lungs. Toxicol. Appl. Pharmacol. 157 (3), 178–191.
Roedel, E.Q., Cafasso, D.E., Lee, K.W.M., Pierce, L.M., 2012. Pulmonary toxicity after exposure to military-relevant heavy metal tungsten alloy particles. Toxicol. Appl. Pharmacol. 259 (1), 74–86.
Roth, D.M., Swaney, J.S., Dalton, N.D., Gilpin, E.A., Ross Jr., J., 2002. Impact of anesthesia on cardiac function during echocardiography in mice. Am. J. Physiol. Heart Circ. Physiol. 282 (6), H2134–H2140.
Schröder, K., Vecchione, C., Jung, O., Schreiber, J.G., Shiri-Sverdlov, R., van Gorp, P.J., Busse, R., Brandes, R.P., 2006. Xanthine oxidase inhibitor tungsten prevents the development of atherosclerosis in ApoE knockout mice fed a Western-type diet. Free Radic. Biol. Med. 41 (9), 1353–1360.
Shiue, I., Hristova, K., 2014. Higher urinary heavy metal, phthalate and arsenic concentrations accounted for 3-19% of the population attributable risk for high blood pressure: US NHANES, 2009-2012. Hypertens. Res. 37 (12), 1075–1081.
Shvedova, A.A., Kisin, E.R., Yanamala, N., Farcas, M.T., Menas, A.L., Williams, A., Fournier, P.M., Reynolds, J.S., Gutkin, D.W., Star, A., Reiner, R., Halappanavar, S., Kagan, V.E., 2015. Gender differences in murine pulmonary responses elicited by cellulose nanocrystals. Part. Fibre Toxicol. 13 (1), 28.
Stefaniank, A.B., Virji, M.A., Day, G.A., 2009. Characterization of exposures among cemented tungsten carbide workers. Part I: size-fractionated exposures to airborne cobalt and tungsten particles. J. Expo. Sci. Environ. Epidemiol. 19 (5), 475–491.
Tajima, S., Ikeda, Y., Enomoto, H., Imao, M., Horinouchi, Y., Izawa-Ishizawa, Y., Kihira, Y., Miyamoto, L., Ishizawa, K., Tsuchiya, K., Tamaki, T., 2015. Angiotensin II alters the expression of duodenal iron transporters, hepatic hepcidin, and body iron distribution in mice. Eur. J. Nutr. 54 (5), 709–719.
Templeton, S., McVeigh, C.M., Nguyen, C., Hunter, R., Scieszka, D., Herbert, G.W., Barr, E.B., Liu, R., Gu, H., Bleske, B.E., Campen, M.J., Bolt, A.M., 2023. Acute inhalation of tungsten particles results in early signs of cardiac injury. Toxicol. Lett. 384, 52–62.
Tyrrell, J., Galloway, T.S., Abo-Zaid, G., Melzer, D., Depledge, M.H., Osborne, N.J., 2013. High urinary tungsten concentration is associated with stroke in the National Health and nutrition examination survey 1999–2010. PloS One 8, 1–7.

Villalba-Orero, M., Garcia-Pavia, P., Lara-Pezzi, E., 2022. Non-invasive assessment of HFpEF in mouse models: current gaps and future directions. BMC Med. 20 (1), 349.
Wessling-Resnick, M., 2017. Excess iron: considerations related to development and early growth. Am. J. Clin. Nutr. 106 (Suppl. 6), 1600S–1605S.
Wikström, J., Grönros, J., Gan, L.M., 2008. Adenosine induces dilation of epicardial coronary arteries in mice: relationship between coronary flow velocity reserve and coronary flow reserve in vivo using transthoracic echocardiography. Ultrasound Med. Biol. 34 (7), 1053–1062.
World Health Organization. Hypertension Facts Sheet. March 16th, 2023 Online Access. https://www.who.int/news-room/fact-sheets/detail/hypertension. Last Accessed: September 1st 2025.
Yaeger, M.J., Reece, S.W., Kilburg-Basnyat, B., Hodge, M.X., Pal, A., Dunigan-Russell, K., Luo, B., You, D.J., Bonner, J.C., Spangenburg, E.E., Tokarz, D., Hannan, J., Armstrong, M., Manke, J., Reisdorph, N., Tighe, R.M., Shaikh, S.R., Gowdy, K.M., 2021. Sex differences in pulmonary eicosanoids and specialized pro-resolving mediators in response to ozone exposure. Toxicol. Sci. 183 (1), 170–183.
Zhao, S., Fan, L., Wang, Y., Dong, S., Han, M., Qin, Y., Chen, J., Liu, A., 2023. Combined exposure to multiple metals on hypertension in NHANES under four statistical models. Environ. Sci. Pollut. Res. Int. 30 (40), 92937–92949.